Journal of Orthopaedic Translation (2019) 16, 62—70

Available online at www.sciencedirect.com

ScienceDirect

journal homepage: http://ees.elsevier.com/jot

ORIGINAL ARTICLE

Use of a three-dimensional printed polylactide-coglycolide/tricalcium phosphate composite scaffold incorporating magnesium powder to enhance bone defect repair in rabbits

Wen Yu [a,e,☆], Rui Li [a,☆], Jing Long [b], Peng Chen [a], Angyang Hou [a], Long Li [b], Xun Sun [a], Guoquan Zheng [d], Haoye Meng [a], Yu Wang [a], Aiyuan Wang [a], Xiang Sui [a], Quanyi Guo [a], Sheng Tao [d], Jiang Peng [a], Ling Qin [b,c,**], Shibi Lu [a,*], Yuxiao Lai [b,***]

[a] *Lab of Orthopaedics of Department of Orthopaedics, Chinese PLA General Hospital, Beijing Key Lab of Regenerative Medicine in Orthopaedics, Key Lab of Musculoskeletal Trauma & War Injuries of PLA, Beijing 100853, PR China*
[b] *Translational Medicine R&D Center, Institute of Biomedical and Health Engineering, Shenzhen Institutes of Advanced Technology, Chinese Academy of Sciences, Shenzhen 518057, PR China*
[c] *Musculoskeletal Research Lab of Department of Orthopaedics & Traumatology and Innovative Orthopaedic Biomaterial and Drug Translational Research Laboratory of Li Ka Shing Institute of Health, The Chinese University of Hong Kong, Hong Kong SAR, PR China*
[d] *Department of Orthopaedics, Chinese PLA General Hospital, Beijing 100853, PR China*
[e] *Department of Orthopaedics, 307 Hospital of PLA, Beijing 100071, PR China*

Received 27 April 2018; received in revised form 18 July 2018; accepted 23 July 2018
Available online 16 August 2018

KEYWORDS
Additive manufacture;

Abstract *Background:* The repair of large bone defects remains challenging for orthopaedic surgeons. Bone grafting remains the method of choice; such grafts fill spaces and enhance bone repair. Therapeutic agents also aid bone healing. The objective of this study is to develop a

* Corresponding author. Lab of Orthopaedics of Department of Orthopaedics, Chinese PLA General Hospital, Beijing Key Lab of Regenerative Medicine in Orthopaedics, Key Lab of Musculoskeletal Trauma & War Injuries of PLA, Beijing 100853, PR China.
** Corresponding author. Musculoskeletal Research Lab of Department of Orthopaedics & Traumatology and Innovative Orthopaedic Biomaterial and Drug Translational Research Laboratory of Li Ka Shing Institute of Health, The Chinese University of Hong Kong, Hong Kong SAR, PR China.
*** Corresponding author. Translational Medicine R&D Center, Institute of Biomedical and Health Engineering, Shenzhen Institutes of Advanced Technology, Chinese Academy of Sciences, Shenzhen 518057, PR China.
E-mail addresses: lingqin@cuhk.edu.hk (L. Qin), lushibi301@126.com (S. Lu), yx.lai@siat.ac.cn (Y. Lai).
☆ Wen Yu and Rui Li were co-first authors.

https://doi.org/10.1016/j.jot.2018.07.007

Bone scaffold;
Magnesium;
Osteogenesis;
Segmental bone defect

composite bioactive scaffold composed of polylactide-coglycolide (PLGA) and tricalcium phosphate (TCP) (the basic carrier) incorporating osteogenic, bioactive magnesium metal powder (Mg).
Method: Porous PLGA/TCP scaffolds incorporating Mg were fabricated using a low-temperature rapid-prototyping process. We term the PLGA/TCP/Mg porous scaffold (hereafter, PPS). PLGA/TCP lacking Mg served as the control material when evaluating the efficacy of PPS. A total of 36 New Zealand white rabbits were randomly divided into blank, PLGA/TCP (P/T) and PPS group, with 12 rabbits in each group. We established bone defects 15 mm in length in rabbit radii to evaluate the *in vivo* osteogenic potential of the bioactive scaffold in terms of the direct controlled release of osteogenic Mg ion during *in vivo* scaffold degradation. Radiographs of the operated radii were taken immediately after implantation and then at 2, 4, 8 and 12 weeks. Micro-computed tomography of new bone formation and remaining scaffold and histological analysis were performed at 4, 8, 12 weeks after operation.
Results: X-ray imaging performed at weeks 4, 8 and 12 post-surgery revealed more newly formed bone within defects implanted with PPS and PLGA/TCP scaffolds than blank group ($p < 0.05$). And micro-computed tomography performed at weeks 4 and 8 after surgery revealed more newly formed bone within defects implanted with PPS scaffolds than PLGA/TCP scaffolds ($p < 0.05$). Histologically, the PPS group had more newly mineralized bone than controls ($p < 0.05$). The increases in new bone areas (total implant regions) in the PPS and PLGA/TCP groups were 19.42% and 5.67% at week 4 and 48.23% and 28.93% at week 8, respectively. The percentages of remaining scaffold material in total implant regions in the PPS and PLGA/TCP groups were 53.30% and 7.65% at week 8 and 20.52% and 2.70% at week 12, respectively.
Conclusion: Our new PPS composite scaffold may be an excellent orthopaedic substitute; it exhibits good biocompatibility and may potentially have clinical utility.
Translational potential of this article: Magnesium and beta-tricalcium phosphate had osteoinduction. It is significant to print a novel bone composite scaffold with osteoinduction to repair segmental bone defects. This study evaluated efficacy of PPS in the rabbit radius segmental bone defect model. The results showed that the novel scaffold with good biocompatibility may be an excellent graft and potentially have clinical utility.

Introduction

Repair of segmental bone defects caused by trauma, infection, tumours and other conditions is orthopaedically challenging because bone regeneration potential is low with or without bone grafting. Improved osteogenesis of bone grafts and reductions in the amounts of autologous bone required are urgently needed. Bioceramics, such as calcium phosphate, exhibit good bioactivity, biodegradability and biocompatibility and serve as efficient and safe bone repair materials [1,2]. Magnesium has recently been reported to constitute an excellent biodegradable orthopaedic implant, heralding potential applications in terms of fixation of bone fractures and treatment of pseudoarthrosis [3,4]. Mg is essential for bone health [5,6]. Mg is bioactive and exhibits the mechanical strength required for bone healing. The use of additive manufacturing technologies by bone tissue engineers has greatly accelerated research on and development of bone regeneration [7,8].

Scaffold biomaterials have various orthopaedic applications [9]. Polymeric materials such as polylactide-coglycolide (PLGA) can be dissolved in organic solvents to form pastes and then serve as basic biomaterials for the formation of porous three-dimensional (3D) scaffolds by spinning technology with the addition of tricalcium phosphate (TCP), which buffers the low pH associated with PLGA degradation, reducing inflammation and enhancing the mechanical properties of the scaffold [10—13]. In the present study, PLGA and TCP served as carriers for the fabrication of composite porous scaffolds incorporating Mg (PLGA/TCP/Mg porous scaffolds; hereafter, PPSs) by established, low-temperature rapid-prototyping technology [14—18]. As Mg has an osteogenic effect that is useful for orthopaedic applications, Mg incorporation into PLGA/TCP to form composite porous scaffolds may encourage research on and development of biomaterials incorporating a relevant bioactive metal [18,19]. We recently showed that implant-derived Mg induced local neuronal production of calcitonin gene-related peptide, improving osteoporotic fracture healing in rats [20]. In the present study, we further investigated bone repair augmentation by Mg, using a standard, rabbit, radial segmental defect model. We systemically evaluated bone repair using radiography and micro-computed tomography (micro-CT) and histologically.

Materials and methods

Preparation of composite bioactive scaffolds

Porous PLGA/TCP scaffolds incorporating Mg were fabricated by a low-temperature rapid-prototyping process (CLRF-2000-II instrument, Tsinghua University, China) following an established protocol [18,21]. Briefly, PLGA and TCP powders

(weight ratio 4:1) were dissolved in 1,4-dioxane to form a homogeneous solution. PLGA was added according to the recommended powder weight:solution volume ratio of 13:100. The Mg:TCP ratio was 2:1, similar to that used in a recent *in vitro* study [21]. Because 1,4-dioxane is volatile, it was completely removed over 24 hours of freeze-drying at an ice condenser temperature of −30°C and a negative pressure of 500 Pa. All scaffolds were trimmed to $3 \times 3 \times 15$ mm^3 for fitting into bone defects.

Characterization of PT and PPS scaffolds

Morphology and porosity

The longitudinal surface morphologies of the scaffolds were examined using a scanning electron microscope (SEM; JSM-6390; JEOL, Tokyo, Japan) operating at 15 kV and 5.0 mA. The average pore size was determined by analysing micrographs. Porosities were measured using micro-CT.

In vitro cytocompatibility

MC3T3-E1 osteoblastic cells (Subclone 14, CRL-2594) were purchased from the American Type Culture Collection, Manassas, VA, USA, and used to investigate *in vitro* scaffold cytocompatibilities. Cells were cultured in α-Modified Eagle Medium (α-MEM) (Hyclone, Thermo Scientific, USA) supplemented with 10% (v/v) foetal bovine serum (GibcoBRL, Grand Island, NY, USA) and a 1% (w/v) antibiotic solution (100 U/mL penicillin and 100 mg/mL streptomycin sulphate; GibcoBRL) at 37°C in a humidified atmosphere under 5% (v/v) CO_2; the culture medium was changed every 3 days.

A cell-counting kit-8 assay was used to measure cell adhesion to scaffolds after 6, 12 and 24 hours. Cells were seeded at 6×10^4/cm^2 into a 48-well plate containing scaffold samples (α-MEM served as the negative control) followed by coincubation at 37°C in a humidified atmosphere under 5% (v/v) CO_2. At each time point, 40 μL of cell-counting kit-8 solution (Dojindo Molecular Technologies Inc., Kumamoto, Japan) was added to each well, followed by incubation for 3 hours at 37°C; then, optical density (OD) values were read at 450 nm and 620 nm using a microplate reader (Synergy HT, BioTek, USA). The mean ODs of the negative controls were subtracted from the ODs of the test groups. Cell proliferation was also explored at 1, 3 and 7 days. Cells were seeded at 2×10^4/cm^2. The OD values on days 3 and 7 were normalised to those on day 1.

In vitro assessment of osteogenesis

MC3T3-E1 cells were obtained and cultured in the same way. Four different scaffolds were prepared, PLGA, PLGA/5% Mg (mass fraction of Mg is 5%), PLGA/10% Mg and PLGA/15% Mg. The cells (2×10^5) were planted on each scaffold, and β-glycerol phosphate (10 mM) and ascorbic acid (50 μg/mL) were added into the basic medium. Refreshing the differentiation medium every 3 days, after induction of differentiation medium for 28 days, alizarin red staining was performed, and the results are shown in Figure S1.

Establishment of radial segmental defects in rabbits

We created segmental, radial bone defects in adult male New Zealand white rabbits [22—25]. A 15 mm segment of the radius midshaft was surgically removed to create a critically sized defect (Fig. 1A). Right mid-radius osteotomies were performed on 3.5-month-old New Zealand white male rabbits weighing 2—2.5 kg [26]. Two types of scaffolds were tested, the pure PLGA/TCP scaffold (control) and the test PPS scaffold (Fig. 1B). A total of 36 forelimbs (four samples per time point) of 36 rabbits were divided into three groups, with 12 forelimbs in each group. Twelve forelimbs were subjected to decalcification and histological examination (four at each of weeks 4, 8 and 12). Defect healing was monitored in all 36 rabbits by X-ray imaging at weeks 2, 4, 8 and 12 and by micro-CT at weeks 4, 8 and 12.

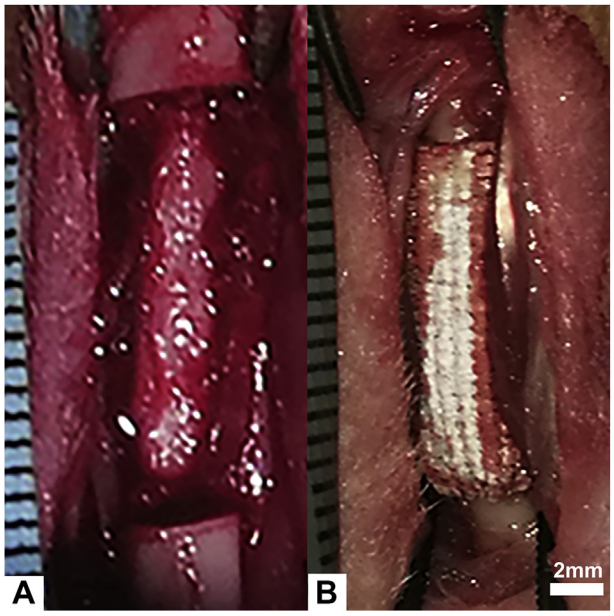

Fig. 1 Creation of radial segmental bone defects in rabbits and implantation of porous composite scaffolds. (A) Fifteen-millimeter defects were created in the midshafts of adult New Zealand white rabbits; (B) PLGA/TCP-based porous scaffold with size $3 \times 3 \times 15$ mm^3 was implanted into the defect region. PLGA = polylactide-coglycolide; TCP = tricalcium phosphate.

Under general anaesthesia (ketamine 2 mg kg^{-1} body weight and xylazine hydrochloride 50 mg kg^{-1} body weight; 1:1 v/v), the right forelimbs were shaved and prepared with povidone; then, 20 mm long incisions were created above the radii. The soft tissue was resected, and a 15 mm segment of each radius was removed using an oscillating saw (Synthes; Mathys AG, Bettlach, Switzerland) followed by saline irrigation. Scaffolds were press-fitted into the radial defects, and the wounds were flushed with saline and closed with several layers of sutures. Pain was managed via postsurgery injections of Temgesic three times over the first 72 hours; benzylpenicillin sodium was injected on each of the following 7 days to prevent infection. Animals were allowed free access to food and water, and movement was not restricted. The animal experimental ethics committee of the corresponding author's institution approved the study protocol.

Radiography and evaluation of new bone areas

High-resolution radiographs of the radii were taken immediately after implantation (baseline) and on postoperative

weeks 2, 4, 8 and 12 using a machine made by the Faxitron X-ray Corporation, USA. The exposure time was 10 seconds, the tube voltage was 58 kV and the magnification was 1.5×. All images were saved in tagged image file format (TIFF) format. Newly formed bone was quantified in terms of size and area using the Image-Pro Plus software, version 6.0 (Media Cybernetics, USA). New bone evident in radiographs of each time point was graded 1—4 [i.e., area fraction of new bone: 0—25% (1); 25—50% (1—2); 50—75% (2—3) and 75—100% (3—4)] [27].

CT evaluation

At the postoperative time points mentioned previously, newly formed bone was evaluated by micro-CT (GE, USA) using a published protocol [28]. Briefly, all defect regions were scanned at a spatial resolution of 45 μm, and the bony compartments were segmented from marrow and soft tissue for subsequent analyses using the global threshold procedure. A threshold of 1200 reflected bony tissue, and thresholds <1200 reflected marrow, soft tissue and the implanted composite scaffolds [29]. New bone was evaluated in terms of bone mineral density (BMD), tissue volume (TV), bone volume (BV). And remaining scaffold volume (SV) was also evaluated.

Histological evaluation

After micro-CT evaluation, all samples were fixed in 4% (v/v) paraformaldehyde (pH 7.2) for 24 hours, decalcified in ethylenediaminetetraacetic acid at 37°C for 2 months, dehydrated in an automatic tissue hydroextractor (Leica-ASP200S, Germany) and embedded in paraffin using an embedder (BMJ-1; Tianjin Tianli Aviation Electromechanical, China). Fine-micrometre-thick sections were prepared along the radial long axes and coronal planes using a microtome (Leitz model 1516; Germany). Serial sections were stained using two methods, as described in the following, before microscopic evaluation.

Statistical analyses

All quantitative data are presented as means ± standard deviations (SDs). Data were compared using two-way analysis of variance, and bone marrow recanalisation rates were compared using the Chi square test with SPSS software, version 22.0 (SPSS, Chicago, IL, USA). Statistical significance was set to $p < 0.05$.

Results

All rabbits survived to the end of the experiment. No postoperative fractures or infections were noted.

Scaffold morphologies and porosities

Photographs and SEM images of the PPS scaffolds are shown in Figure 2. The macropore diameter was about 450 μm. The porosities were >85% and 76%, respectively. The connectivities of both scaffolds were almost 100%. Phase separation revealed many micropores (2.5—90 μm in diameter) on the scaffold walls.

In vitro cytocompatibility

The results of *in vitro* cytocompatibility testing are shown in Figure 3. ODs reflect the numbers of cells adhering to specimen surfaces. Significantly more cells were adhering to PLGA/TCP scaffold than PPS scaffold at 6, 12 and 24 hours (Fig. 3A, $p < 0.01$). The proliferation rate of cells of PLGA/TCP was higher than the rates of PPS at 3 and 7 days (Fig. 3B, $p < 0.01$).

In vitro assessment of osteogenesis

After induction of differentiation medium for 28 days, calcium nodules were formed in three kinds of Mg-containing scaffolds, which was confirmed by alizarin red staining. But PLGA/15% Mg scaffold formed the most calcium nodules (Figure S1).

Radiographic area fractions of new bone within defects

As shown in Figure 4, defects that were not filled with scaffold contained scattered bony structures, and the bony ends gradually closed commencing at 4 weeks. After implantation of PLGA/TCP scaffolds and PPSs, complete bridging of the bony ends was evident along the border of

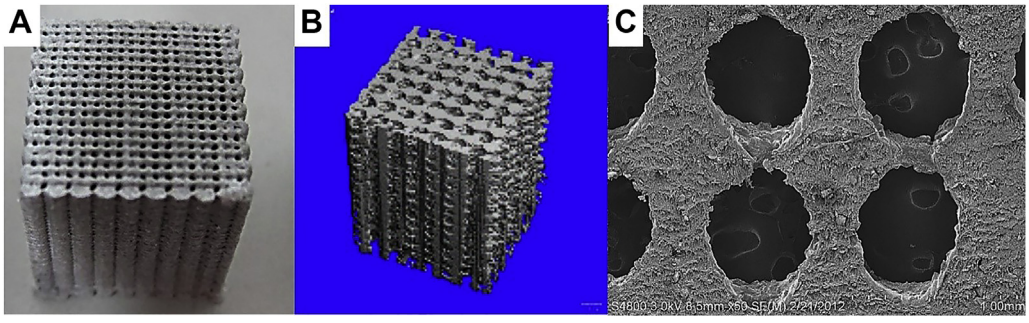

Fig. 2 Morphologies of the PPS. (A) Photograph of the PPS; (B) CT micrograph of the PPS; (C) A representative SEM image of the PPS (50×).
CT = computed tomography; PLGA = polylactide-coglycolide; PPS = PLGA/TCP/Mg porous scaffold; SEM = scanning electron microscope; TCP = tricalcium phosphate.

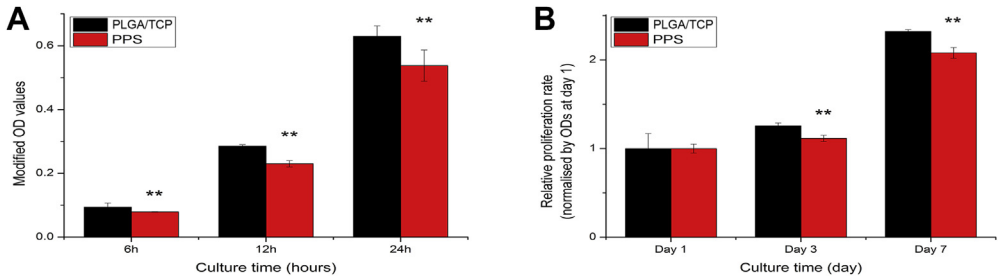

Fig. 3 Adhesion and proliferation of MC3T3-E1 cells on the scaffolds: (A) Cell adhesion at 6, 12 and 24 hours; (B) Cell proliferation at 1, 3 and 7 days. The modified OD values are the ODs at 450 nm minus the ODs at 620 nm. The modified OD values at 3 and 7 days were normalized to those at 1 day. $^{**}p < 0.01$.

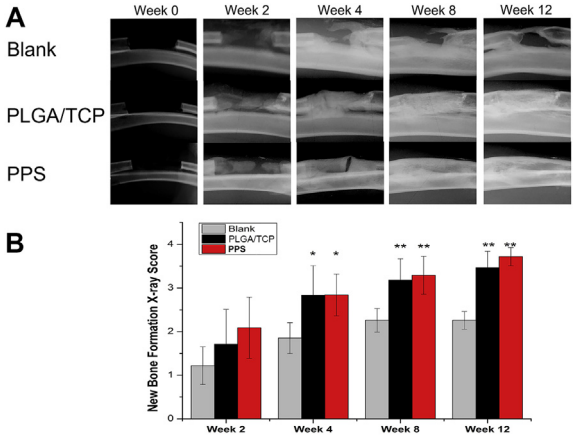

Fig. 4 (A) Representative radiographs of radial segmental defects implanted or not with porous scaffolds taken at weeks 0 (baseline), 2, 4, 8 and 12 postoperatively. The P/T and PPS groups exhibited more bone-filling than the control. (B) Mean X-ray scores at weeks 2, 4, 8 and 12 postoperatively. The P/T and PPS groups exhibited more bone formation than the control ($^{*}p < 0.05$, $^{**}p < 0.01$ for comparisons between the P/T and PPS groups and the control at each time point; $n = 6$).
PLGA = polylactide-coglycolide; PPS = PLGA/TCP/Mg porous scaffold; TCP = tricalcium phosphate.

the ulna, extending approximately halfway through the defects. At each evaluation time after operation, the X-ray scores of new bone formation in the PLGA/TCP and PPS groups were higher than those of the control group ($^{*}p < 0.05$, $^{**}p < 0.01$, n = 4), although statistical significance was not attained at the 2-week time point. Moreover (although statistical significance was not attained), at each evaluation time after operation, the X-ray score of new bone formation in the PPS group was greater than that in the PLGA/TCP group (p-values 0.36, 0.98, 0.64 and 0.23 at weeks 2, 4, 8 and 12, respectively). At 12 weeks after operation, the mean percentages of newly formed bone in the defect regions were 56.5% for the control group and 86.8% and 93.0% for the PLGA/TCP and PPS groups, respectively (Figure 4B).

Measurement of newly formed bone via micro-CT

The 3D images obtained after micro-CT reconstruction (Fig. 5A) revealed newly formed bone at weeks 4, 8 and 12 after scaffold implantation. At week 4, the bone volume fraction (BV/TV) of the PPS group was significantly greater than that of the PLGA/TCP group. In addition, the BMD of the PPS group was usually greater than that of the PLGA/TCP group, although statistical significance was not attained at the 4-week time point. At week 8, the BV/TV and BMD of the PPS group were significantly greater than those of the PLGA/TCP group. At week 12, the BMD and BV/TV of the PPS group were lower than those of the PLGA/TCP group, but statistical significance was not attained (Fig. 5B1-2). Moreover, the bone marrow recanalisation rates in the PPS and PLGA/TCP groups were 50% and 0% at week 8 and 100% and 50% at week 12, respectively (Fig. 5B3). The percentage of remaining SV in the PPS group was less than that in the PLGA/TCP group at each time point ($p < 0.05$) (Fig. 5B4). At each time point, the PPS group exhibited more new bone than the control group ($p < 0.05$). At week 12, the PLGA/TCP group exhibited more new bone than the control group ($p < 0.05$); however, at weeks 4 and 8, no significant differences were apparent between the PLGA/TCP and control groups.

Histological analyses of new bone formation

No notable healing was evident up to week 2 after surgery. The scaffold pores were filled with loose fibrous connective tissue. Figure 6 illustrates *in vivo* osteogenesis at weeks 4, 8 and 12. Newly formed woven bone was observed at week 4. At weeks 4 and 8, the PPS group exhibited large bone islands within the scaffolds. Defects lacking implants exhibited only concave fibrous tissue. In defects with scaffolds, newly formed tissue (viable osteocytes within lacunae embedded in a bony matrix) was deposited directly on the porous surfaces, and osteoblast-like cells lined the surface of newly formed bone, creating a bony matrix within the scaffolds.

Haematoxylin and eosin (H&E; Fig. 6) staining revealed new bone growth in the pores of both scaffold groups, which suggests that the scaffolds exhibited good osteoconductivity and osteoinduction.

In addition, Masson's trichrome staining (Fig. 7) revealed significantly more new bone in defects treated with the PPS scaffold (compared to other materials) at week 4 ($p < 0.01$). At week 8, the PPS group also exhibited more new bone formation than the PLGA/TCP group ($p = 0.09$), although statistical significance was not attained. At week 12, the PPS group exhibited less new bone formation than

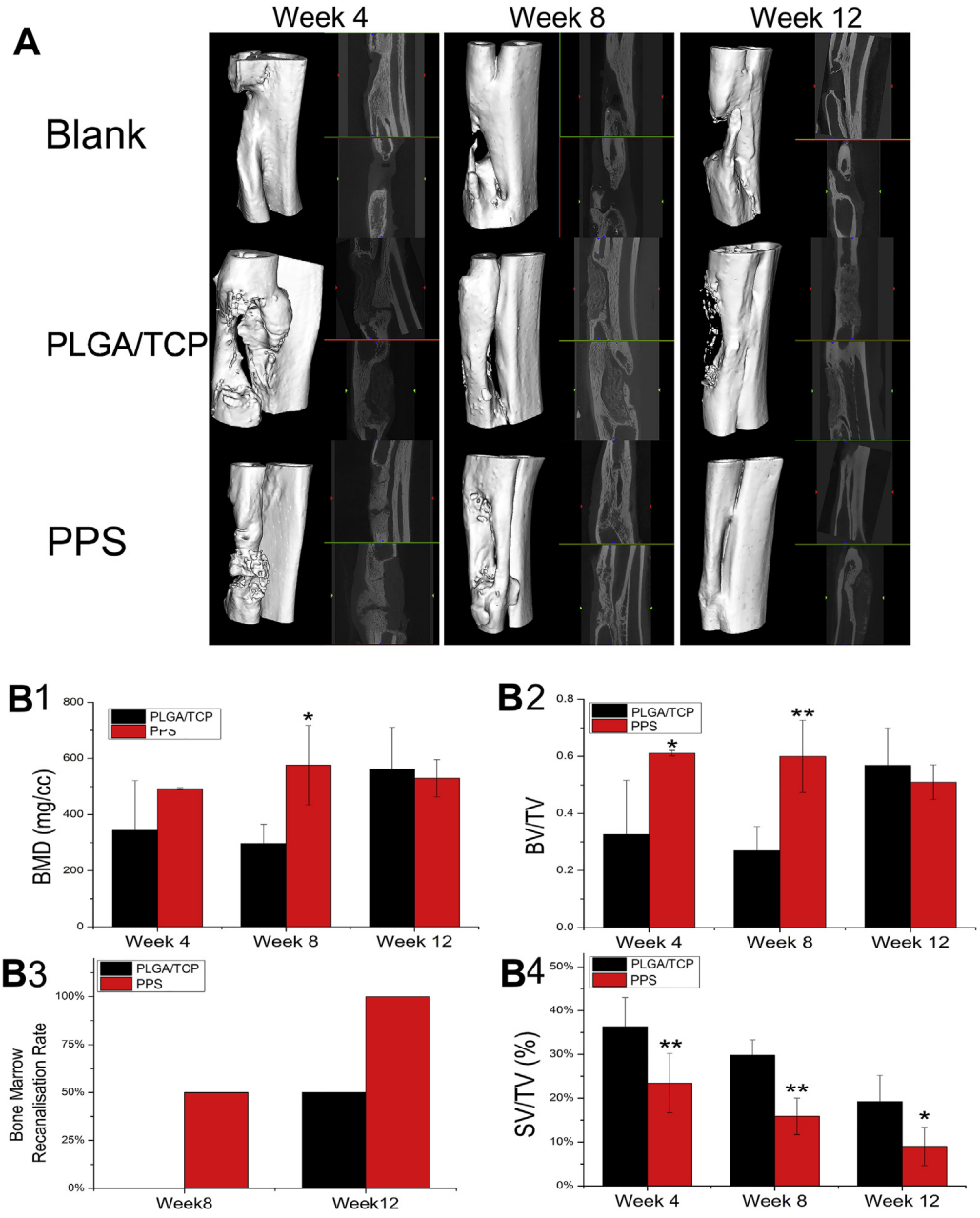

Fig. 5 (A) Representative 3D micro-CT images of the radial segmental defects at weeks 4, 8 and 12 after implantation. The PPS group exhibited more new bone than the control at all three time points. (B) Bone volumes and remaining scaffold volumes in bony defects and the BMDs of implanted scaffolds evaluated by micro-CT at weeks 4, 8 and 12. The BMD of the PPS group was generally higher than that of the P/T group, although statistical significance was not attained at week 4. At week 8, the BV/TV and BMD of the PPS group were significantly greater than those of the P/T group. At weeks 8 and 12, the bone marrow recanalization rates were 50% and 0% and 100% and 50% in the PPS and P/T groups, respectively (*$p < 0.05$, **$p < 0.01$ for comparisons between the PPS and P/T groups at each time point; $n = 4$).
BMD = bone mineral density; BV/TV = bone volume fraction; CT = computed tomography; PLGA = polylactide-coglycolide; PPS = PLGA/TCP/Mg porous scaffold; TCP = tricalcium phosphate.

the PLGA/TCP group. In addition, the percentages of remaining scaffold material in the implantation area of the PPS group were lower than those of the PLGA/TCP group at weeks 4, 8, and 12; however, only the differences at weeks 8 and 12 were statistically significant.

From weeks 4–12, new bone wrapped around the scaffold, gradually changed to lamellar bone, formed marrow cavities of various sizes and became gradually fused.

Discussion

We evaluated a unique, biodegradable, PLGA/TCP-based porous scaffold incorporating pure Mg powder in terms of enhancement of bone regeneration within segmental radial defects in rabbits. The scaffold materials did not inhibit *in vitro* bone marrow stromal cell (BMSC) proliferation [30].

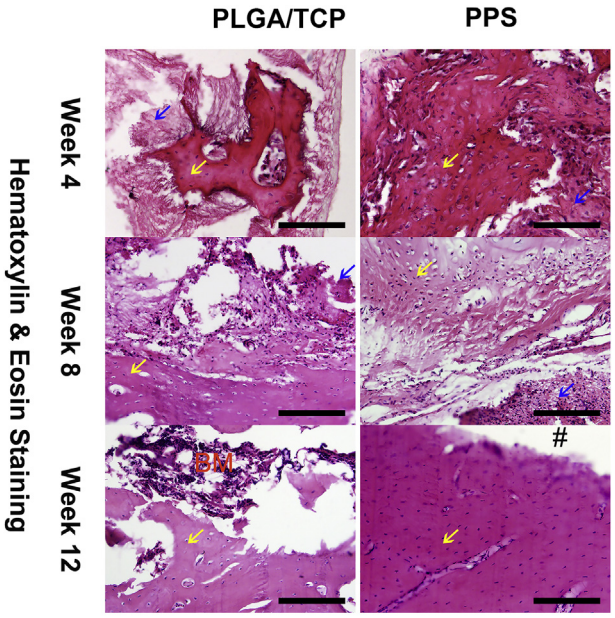

Fig. 6 Representative sagittal sections of decalcified, radial segmental bone defects. Newly formed bone is evident in the PPS and PLGA/TCP groups (H&E staining; blue arrows, scaffold; yellow arrows, new bone; orange capital letters "BM", bone marrow tissue; black hashes, bone marrow cavity; bar = 100 μm).
H&E = Haematoxylin and eosin; PLGA = polylactide-coglycolide; PPS = PLGA/TCP/Mg porous scaffold; TCP = tricalcium phosphate.

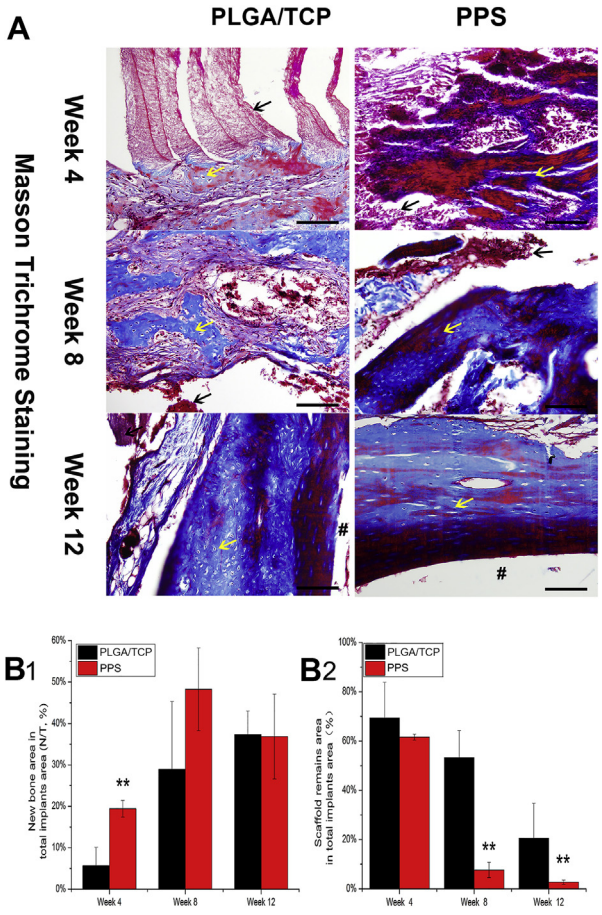

Fig. 7 Representative sagittal sections of decalcified histology of radius segmental bone defects. (A) Masson trichrome staining of sections at week 4 revealed more new bone growth (yellow arrows) in the PPS scaffold than in the PLGA/TCP group (black arrow, scaffold; yellow arrow, new bone; black hashes, bone marrow cavity; bar = 100 μm). (B) New bone areas and remaining scaffold areas at weeks 4, 8 and 12. (**$p < 0.01$ for comparisons between the PPS and PLGA/TCP groups at each time point; $n = 4$).
PLGA = polylactide-coglycolide; PPS = PLGA/TCP/Mg porous scaffold; TCP = tricalcium phosphate.

This is not surprising; both PLGA and TCP are medical-grade materials used in clinical applications. Mg is osteogenic [18,19], and we incorporated Mg into a scaffold before evaluation of biocompatibility and biosafety *in vivo*, a necessary preliminary test when clinical applications are planned. When MC3T3-E1 cells were planted on scaffolds, significantly more cells were observed in PLGA/TCP group than those in PPS group. The most likely reason was that Mg-containing scaffold was slightly toxic to cells. We monitored bone healing via X-ray imaging, micro-CT and *ex vivo* histology, with a focus on the osteogenic potential of a PLGA/TCP scaffold incorporating Mg powder. Radiography showed that, compared to the control, scaffold implantation triggered bone formation 4, 8 and 12 weeks later. Micro-CT showed that, compared to the PLGA/TCP group, the PPS group exhibited more bone formation at weeks 4 and 8. The reason was that Mg ions released by composite scaffold made the local microenvironment alkaline and enhanced the activity of osteoblasts [31]. Therefore, more new bone was formed at 4 and 8 weeks after scaffold implantation, and the callus was formed more quickly. Then, callus remodelling progresses rapidly. When long bone callus was remodelled completely, new bone cortex and marrow cavity were formed, and the new bone in Mg-containing group was less than that of PLGA/TCP group at 12 weeks. However, as bone remodelling progressed, the PPS group exhibited less new bone at week 12 than the PLGA/TCP group but a higher marrow recanalisation rate, although the statistical significance of the latter observation cannot be assessed because of the small sample size. Thus, PLGA/TCP scaffolds are suitable basic biomaterials for incorporation of Mg powder, forming bioactive, porous composite scaffolds.

The PLGA/TCP composite scaffolds facilitated new bone formation and growth. Polymer/ceramic composites are mechanically strong, and their pore sizes and degradation rates favour new bone formation and vessel ingrowth [32—34]. The mechanical properties and degradation rates of scaffolds are both important when developing bone substitutes. During healing after scaffold implantation, scaffold trabeculae are degraded and replaced by new bone, marrow and fibrous connective tissue over time, accompanied by new bone formation and gradual scaffold replacement. The scaffold trabeculae provide the mechanical strength and space required for the formation of new tissue. Biocompatibility is also

very important when evaluating biomaterials. PPS facilitated cell adhesion and proliferation. We implanted both PLGA/TCP scaffolds and PLGA/TCP scaffolds containing Mg powder (of macropore sizes 450 μm and porosities >85%) into bone defects 15 mm in length. Micro-CT and histological results showed that new bone grew or migrated into the scaffold centres through the macropores, and the PPS group exhibited better osteogenic results than both the control and the PLGA/TCP group. Histologically, compared to the PLGA/TCP group, the PPS group exhibited more osteoid tissue and mineralised and mature lamellar bone at weeks 4 and 8, which indicates that the use of PPS may assist bone repair. The release of Mg ion from PPS could enhance bone healing [20,35,36]. The PPS was degraded more rapidly than the PLGA/TCP scaffold at weeks 8 and 12, as reflected by the percentages of residual SVs revealed by micro-CT, which indicates that the local microenvironment favoured rapid new bone formation with replacement of the scaffold.

Our study had certain limitations. The histomorphometrical data exhibited more variation than the micro-CT-based volumetric quantifications of new bone formation. A larger sample size would have rendered the statistical analyses more robust.

Conclusion

We developed a new, composite bioactive scaffold combining Mg powder with PLGA/TCP to enhance bone regeneration in segmental bone defects and investigated its utility *in vivo*. As Mg is biocompatible, PPSs exhibited the desired osteogenic potential in radial bone segmental defects in rabbits. The scaffold exhibited good biocompatibility and may find clinical applications.

Conflicts and interest

The authors have no conflict of interests to declare.

Acknowledgement/Funding

This study was supported by National Key R&D Plan of China (2016YFC1102104), the National Natural Science Foundation of China (NSFC 81603008, 51573206), Beijing Municipal Science and Technology Project (Z161100005016059), Shenzhen Fundamental Research Foundation (Project No. JCYJ20150731154850925), and People's Liberation Army 13th five-year plan period (BWS13C029). Dr. Wen Yu thanks his wife Xiaojuan Su for her wholehearted support of his research work.

Appendix A. Supplementary data

Supplementary data related to this article can be found at https://doi.org/10.1016/j.jot.2018.07.007.

References

[1] Hench LL. The future of bioactive ceramics. J Mater Sci Mater Med 2015;26(2):86 [eng].
[2] Wen Y, Xun S, Haoye M, Baichuan S, Peng C, Xuejian L, et al. 3D printed porous ceramic scaffolds for bone tissue engineering: a review. Biomater Sci 2017;5(9):1690—8.
[3] Witte F. The history of biodegradable magnesium implants: a review. Acta Biomater 2010;6(5):1680—92 [eng].
[4] Zhao D, Huang S, Lu F, Wang B, Yang L, Qin L, et al. Vascularized bone grafting fixed by biodegradable magnesium screw for treating osteonecrosis of the femoral head. Biomaterials 2016;81:84—92 [eng].
[5] de Baaij JH, Hoenderop JG, Bindels RJ. Magnesium in man: implications for health and disease. Physiol Rev 2015;95(1):1—46 [eng].
[6] Li FY, Chaigne-Delalande B, Kanellopoulou C, Davis JC, Matthews HF, Douek DC, et al. Second messenger role for Mg2+ revealed by human T-cell immunodeficiency. Nature 2011;475(7357):471—6 [eng].
[7] Costa PF, Vaquette C, Baldwin J, Chhaya M, Gomes ME, Reis RL, et al. Biofabrication of customized bone grafts by combination of additive manufacturing and bioreactor know-how. Biofabrication 2014;6(3), 035006 [eng].
[8] Wang X, Xu S, Zhou S, Xu W, Leary M, Choong P, et al. Topological design and additive manufacturing of porous metals for bone scaffolds and orthopaedic implants: a review. Biomaterials 2016;83:127—41 [eng].
[9] Place ES, Evans ND, Stevens MM. Complexity in biomaterials for tissue engineering. Nat Mater 2009;8(6):457—70 [eng].
[10] Ehrenfried LM, Patel MH, Cameron RE. The effect of tricalcium phosphate (TCP) addition on the degradation of polylactide-co-glycolide (PLGA). J Mater Sci Mater Med 2008;19(1):459—66 [eng].
[11] Zhang M, James FG, Qin L, Lei M, Chen SH, Xie XH, et al. Comparative study of PLGA/TCP scaffolds incorporated or coated with osteogenic growth factors for enhancement of bone regeneration. J Orthop Transl 2014;2:91—104.
[12] Qin L, Yao D, Zheng L, Liu WC, Liu Z, Lei M, et al. Phytomolecule icaritin incorporated PLGA/TCP scaffold for steroid-associated osteonecrosis: proof-of-concept for prevention of hip joint collapse in bipedal emus and mechanistic study in quadrupedal rabbits. Biomaterials 2015;59:125—43.
[13] Lai Y, Cao H, Wang X, Chen S, Zhang M, Wang N, et al. Porous composite scaffold incorporating osteogenic phytomolecule icariin for promoting skeletal regeneration in challenging osteonecrotic bone in rabbits. Biomaterials 2018;153:1—13.
[14] Chen SH, Wang XL, Xie XH, Zheng LZ, Yao D, Wang DP, et al. Comparative study of osteogenic potential of a composite scaffold incorporating either endogenous bone morphogenetic protein-2 or exogenous phytomolecule icaritin: an in vitro efficacy study. Acta Biomater 2012;8(8):3128—37 [eng].
[15] Kai H, Wang X, Madhukar KS, Qin L, Yan Y, Zhang R, et al. Fabrication of a two-level tumor bone repair biomaterial based on a rapid prototyping technique. Biofabrication 2009;1(2), 025003 [eng].
[16] Wang X, Yan Y, Pan Y, Xiong Z, Liu H, Cheng J, et al. Generation of three-dimensional hepatocyte/gelatin structures with rapid prototyping system. Tissue Eng 2006;12(1):83—90 [eng].
[17] Chen S, Tang T, Liu Z, Lau P, Xie X, Wang X, et al. Study on osteointegrative properties of a functional gradient tumor bone repair materials in ulna bone defect model of rabbits. Bone 2010;47(Suppl 3). S432-S32.
[18] Ma R, Lai YX, Li L, Tan HL, Wang JL, Li Y, et al. Bacterial inhibition potential of 3D rapid-prototyped magnesium-based

porous composite scaffolds-an in vitro efficacy study. Sci Rep 2015;5, 13775.
[19] Liu YJ, Yang ZY, Tan LL, Li H, Zhang YZ. An animal experimental study of porous magnesium scaffold degradation and osteogenesis. Br J Med Biol Res 2014;47(8):715—20 [eng].
[20] Zhang Y, Xu J, Ruan YC, Yu MK, O'Laughlin M, Wise H, et al. Implant-derived magnesium induces local neuronal production of CGRP to improve bone-fracture healing in rats. Nat Med 2016;22(10):1160—9.
[21] Zhang M, Chen SK, Wang XL, Zhang P. A novel magnesium composed PLGA/TCP porous scaffold for bone regeneration. In: Paper presented at: eCM XIV - stem & progenitor cells for musculoskeletal regeneration; 2013.
[22] Horner EA, Kirkham J, Wood D, Curran S, Smith M, Thomson B, et al. Long bone defect models for tissue engineering applications: criteria for choice. Tissue Eng Part B Rev 2010;16(2):263—71.
[23] Hollinger JO, Kleinschmidt JC. The critical size defect as an experimental model to test bone repair materials. J Craniofac Surg 1990;1(1):60—8 [eng].
[24] Schmitz JP, Hollinger JO. The critical size defect as an experimental model for craniomandibulofacial nonunions. Clin Orthop Relat Res 1986;(205):299—308 [eng].
[25] Li Y, Chen S-K, Li L, Qin L, Wang X-L, Lai Y-X. Bone defect animal models for testing efficacy of bone substitute biomaterials. J Orthop Transl 2015;3(3):95—104.
[26] Bodde EW, Spauwen PH, Mikos AG, Jansen JA. Closing capacity of segmental radius defects in rabbits. J Biomed Mater Res Part A 2008;85(1):206—17 [eng].
[27] Wan C, He Q, Li G. Allogenic peripheral blood derived mesenchymal stem cells (MSCs) enhance bone regeneration in rabbit ulna critical-sized bone defect model. J Orthop Res: Off Publ Orthop Res Soc 2006;24(4):610—8 [eng].
[28] Xue J, Peng J, Yuan M, Wang A, Zhang L, Liu S, et al. NELL1 promotes high-quality bone regeneration in rat femoral distraction osteogenesis model. Bone 2011;48(3):485—95 [eng].
[29] He YX, Zhang G, Pan XH, Liu Z, Zheng LZ, Chan CW, et al. Impaired bone healing pattern in mice with ovariectomy-induced osteoporosis: a drill-hole defect model. Bone 2011;48(6):1388—400 [eng].
[30] Xie XH, Wang XL, Zhang G, He YX, Leng Y, Tang TT, et al. Biofabrication of a PLGA-TCP-based porous bioactive bone substitute with sustained release of icaritin. J Tissue Eng Regen Med 2015;9(8):961—72 [eng].
[31] Shen Y, Liu W, Wen C, Pan H, Wang T, Darvell BW, et al. Bone regeneration: importance of local pH—strontium-doped borosilicate scaffold. J Mater Chem 2012;22(17):8662—70.
[32] Takahashi Y, Tabata Y. Effect of the fiber diameter and porosity of non-woven PET fabrics on the osteogenic differentiation of mesenchymal stem cells. J Biomater Sci Polym Ed 2004;15(1):41—57 [eng].
[33] Roy TD, Simon JL, Ricci JL, Rekow ED, Thompson VP, Parsons JR. Performance of degradable composite bone repair products made via three-dimensional fabrication techniques. J Biomed Mater Res Part A 2003;66(2):283—91 [eng].
[34] Karageorgiou V, Kaplan D. Porosity of 3D biomaterial scaffolds and osteogenesis. Biomaterials 2005;26(27):5474—91 [eng].
[35] Xu TO, Kim HS, Stahl T, Nukavarapu SP. Self-neutralizing PLGA/magnesium composites as novel biomaterials for tissue engineering. Biomed Mater 2018;13(3), 035013.
[36] Lin Z, Wu J, Qiao W, Zhao Y, Wong KHM, Chu PK, et al. Precisely controlled delivery of magnesium ions thru sponge-like monodisperse PLGA/nano-MgO-alginate core-shell microsphere device to enable in-situ bone regeneration. Biomaterials 2018;174:1—16.